RSC Advances

PAPER

View Article Online
View Journal | View Issue

Cite this: *RSC Adv.*, 2018, **8**, 6218

A family of 3d metal clusters based on N–N single bonds bridged quasi-linear trinuclear cores: the Mn analogue displaying single-molecule magnet behavior†

Kai Wang,[a] Shen Tang,[a] Zhao-Bo Hu,[b] Hua-Hong Zou,[b] Xiao-Lu Wang,[b] Yan Li,[a] Shu-Hua Zhang,[a] Zi-Lu Chen[b] and Fu-Pei Liang*[ab]

Received 28th November 2017
Accepted 31st January 2018

DOI: 10.1039/c7ra12844d

rsc.li/rsc-advances

The reactions of the diacylhydrazine ligands *N*,*N*′-bisalicyl-2,6-pyridine dicarbohydrazide (H_6sphz) and *N*,*N*′-bis(3-methoxysalicyl)-2,6-pyridine dicarbohydrazide (H_6msphz) with various 3d metal salts, afforded a series of coordination clusters, namely, $[Mn^{III}_2Mn^{II}(sphz)(acac)_2(CH_3OH)_4]$ (**1**, $acac^-$ = acetylacetone anions), $[Ni^{II}_3(msphz)(Py)_4]$ (**2**, Py = pyridine), $[Cu^{II}_6(sphz)_2(Py)_4]$ (**3**) and $[Cu^{II}_6(msphz)_2(Py)_4]\cdot 2DMF\cdot 2H_2O$ (**4**). Cluster **1** and **2** are single ligand assembled quasi-linear trinuclear structures. Both **3** and **4** consist a pair of quasi-linear $\{Cu_3\}$ cores, which are linked together by two crossed ligands. The adjacent 3d metal ions in all trinuclear cores of **1–4** are bridged by N–N single bonds of ligands, which convey ferromagnetic (FM) interactions between 3d metal centers of **1**, and antiferromagnetic (AFM) interactions between those of **2–4**. In particular, the FM interactions and linear arrangement of mixed-valence Mn centers in **1** result in a large spin ground states value (S_T) of 13/2, as well as single-molecule magnet (SMM) behavior of slow relaxation and hysteresis of magnetization.

Introduction

In the last two decades, impressive growth in the studies of molecular magnetic materials has been initiated by the discovery of some polynuclear 3d clusters that was termed as SMMs.[1] These SMMs exhibit slow magnetic relaxation and hysteresis as the macroscopic magnets below blocking temperature (T_b), affording potential applications in the fields of ultra-high density information storage, molecular spintronics and quantum computation.[2] It is believed that the properties of 3d SMMs are determined by two essential required factors, high spin ground states and strong easy axis-type magnetic anisotropy,[3] which are closely related to intramolecular magnetic interactions and the spatial arrangements of anisotropic 3d metal centers.[4]

The continuous efforts in this field thus achieved many 3d SMMs with various structural topologies.[5] Wherein those with linear or quasi-linear topologies (nuclearity ≥ 3) are one of species attracting particular concerns. Their relatively simple bridging structures are helpful for the deliberate tuning of magnetic interactions. They also facilitate co-linear alignments of anisotropy axes of 3d spins, which might bring significant global anisotropies for the whole systems. All these features are favour of promising SMM properties and special magnetic phenomenon. Typical representative includes a family of quasi-linear $\{Mn^{III}_2Ni^{II}_3\}$ SMMs showing pronounced quantum tunnelling steps in hysteresis loops,[5c] and a linear $\{Co^{II}_3\}$ SMM displaying two magnetic relaxation processes at zero dc bias fields, *etc.*[6] Nevertheless, this species is still rare until now, except above two cases. In Mn clusters family with so many SMM members, there were only three trinuclear and one tetranuclear linear cases reported to show SMM behavior so far as we know (list in Table S1†).[7] Linear SMMs based on other anisotropic 3d centers, such as Co^{II}, Fe^{III} and Ni^{II} ions, were also seldom found in previous literature.[8] Thus, the incorporation of 3d metal ions into linear or quasi-linear SMMs remains to be a meaningful research subject in this field.

On the other hand, to tune the magnetic interactions between 3d ions, the sensible choices of bridging ligands are crucial.[9] The ligands containing N–N bridges are just one kind of versatile candidates. Under the premise of small M–N–N–M torsion angles, they could transmit FM interactions and may result in desirable SMM properties. But these expected results are more achievable for ligands bearing aromatic N–N bridges,

[a]*Guangxi Key Laboratory of Electrochemical and Magnetochemical Functional Materials, College of Chemistry and Bioengineering, Guilin University of Technology, Guilin, 541004, China. E-mail: fliangoffice@yahoo.com*

[b]*State Key Laboratory for the Chemistry and Molecular Engineering of Medicinal Resources, School of Chemistry and Pharmacy, Guangxi Normal University, Guilin, 541004, China*

† Electronic supplementary information (ESI) available: Additional structural figures and magnetic data. Tables of selected bond lengths (Å) and angles (°). CCDC 1496802 and 1496805–1496807. For ESI and crystallographic data in CIF or other electronic format see DOI: 10.1039/c7ra12844d

such as various pyrazoles, triazoles, tetrazoles, *etc.*[10] Those affording saturated N–N single bonds as magnetic exchange pathways, which represented by a variety of acylhydrazines and acylhydrazones, can only transmit AFM interactions between 3d ions in most cases.[11] Up to now, only very limited 3d systems in which N–N single bonds convey FM coupling and/or result in SMM behavior were reported.[8c,12]

In recent years, our group is interested in the coordination chemistry of diacylhydrazine derivatives.[13,14] On the basis of our previous work, we realized that two diacylhydrazine derivatives H_6sphz and H_6msphz, whose chelating pockets preferred by 3d ions arrange in a quasi-linear manner (Scheme 1), might be the right candidates to assemble quasi-linear 3d clusters. We thus started to explore their possibilities in this aspect. Various terminal ligands were also introduced by different ways, so as to block the formation of polymeric products and allow for successful achievement of discrete linear topologies. A family of 3d clusters **1–4** that contain N–N bonds bridged linear trinuclear cores were finally synthesized as we intended. The magnetic investigations revealed the N–N single bonds transmit FM and AFM interactions between the 3d ions of **1** and **2–4**, respectively. Notably, cluster **1** is found to be the rare quasi-linear 3d SMM employing N–N single bonds as magnetic coupling pathways.

Results and discussion

Structural description

X-ray single crystal diffraction revealed that **1** belongs to orthorhombic *Pbcn* space group. As shown in Fig. 1, its centro-symmetric molecular structure contains a $sphz^{6-}$ ligand, three Mn centers, two $acac^-$ ions and four CH_3OH molecules. Bond valence sum (BVS) calculations[15] (3.40 for Mn1 and 1.90 for Mn2) and charge balance consideration established that terminal Mn1 and central Mn2 are trivalent and divalent, respectively. The Mn1 displays a six-coordinated octahedron geometry, whose four equatorial positions are occupied by a $N_{acylhydrazine}$ (N1), an O_{phenol} (O1), an $O_{acylhydrazine}$ (O3) and an O_{acac} (O4) atoms. As expected for high-spin Mn^{3+} ions in an octahedral geometry, an O_{acac} (O5) and an $O_{methanol}$ (O6) atoms locate in two axial positions along a J–T elongation axis, forming two long Mn–O bonds whose lengths are 2.161(2) and 2.347(2) Å, respectively. The central Mn2 residing on an inversion center displays a seven-coordinated pentagonal bipyramid geometry. Its equatorial plane is composed of a N_{Py} (N1), four $N_{acylhydrazine}$ (N2, N3, N2a and N3a) and two

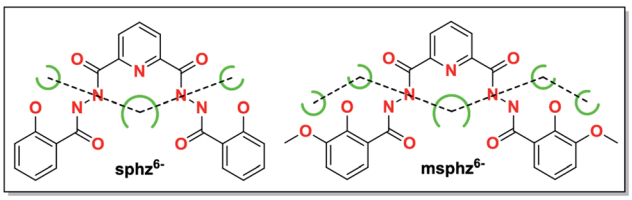

Scheme 1 Potential chelating pockets arranging in quasi-linear fashion for H_6sphz and H_6msphz ligands.

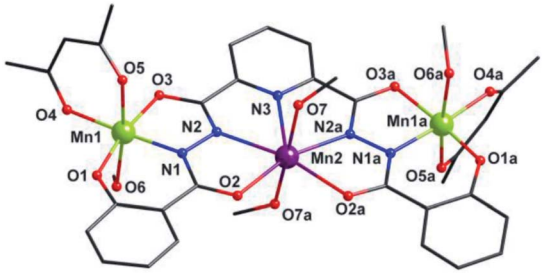

Fig. 1 Molecular structure of **1**. Symmetry codes: (a) $-x, y, -z + 1/2$. Color scheme: black for C, red for O, blue for N, purple for Mn^{2+} ion and grass-green for Mn^{3+} ions.

$O_{acylhydrazine}$ (O3 and O3a) atoms. The axial positions are held by two $O_{methanol}$ (O7 and O7a) atoms with Mn–O bond length of 2.211(2) Å.

Three Mn centers are linked together in a quasi-linear fashion by two N–N single bonds of ligand, which is completely deprotonated and displays an μ_3-η^{11} mode (mode-I in Scheme 2). Two $acac^-$ ions and four CH_3OH act as terminal groups, preventing the formation of infinite expand products. The torsion angle of Mn1–N–N–Mn2 and the Mn1···Mn2 distance are 172.5° and 4.935 Å respectively (Table S2†). The angle of Mn1···Mn2···Mn1a is 153.1°, indicating that three Mn centers are not arranged in a straight line, but remain have a considerable bent angle. However, if seen from *c*-axis direction, three Mn centers and all their donors in equatorial positions are nearly coplanar, with a least-square deviation of 0.092 (Fig. S1†). Note that the J–T axes of two Mn^{3+} ions are nearly co-parallel, and the angle between them is about 6.2°.

Additionally, hydrogen bonds (O6a–H6a···O5b: 2.172 Å; O7a–H7a···O1c: 1.993 Å) are found between the neighboring clusters, which extend the discrete $\{Mn_3\}$ clusters into a 2D supramolecular layer in the *ac* plane (Fig. 2). They may also help to stabilize axially elongated Mn1–O6 (2.347(2) Å) and Mn1–O5 (2.1612(2) Å) bonds, contributing to the formation of +3 oxidation states of Mn1 ions.[16]

Cluster **2** crystallizes in orthorhombic *Pnma* space group. Its $msphz^{6-}$ ligand adopts the same μ_3-η^{11} mode (mode-II, Scheme 2) as $sphz^{6-}$ ligand in **1**, leaving two $O_{methoxyl}$ atoms uncoordinated. Thus **2** also displays a centro-symmetric linear trinuclear

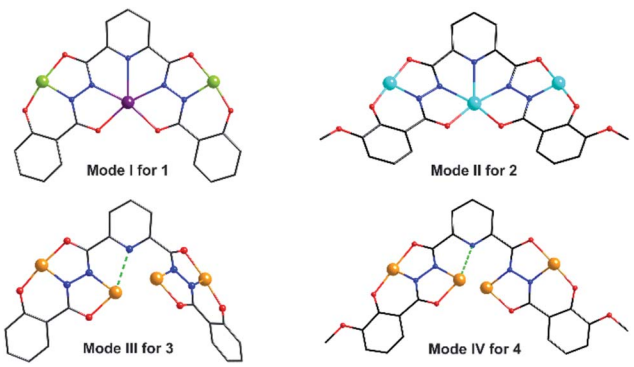

Scheme 2 The coordination modes of the ligands in **1–4**.

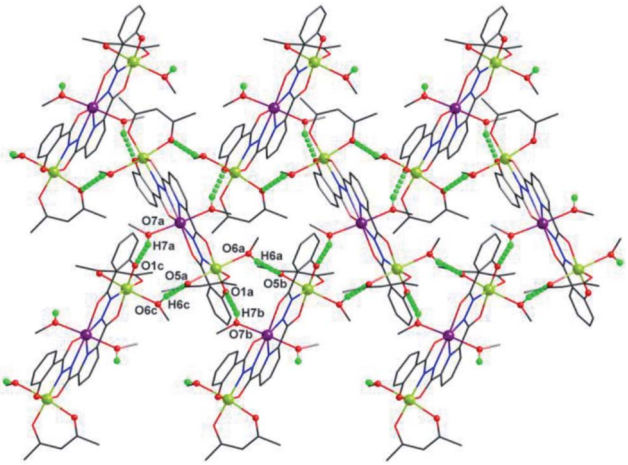

Fig. 2 2D supramolecular layer in *ac* plane linked together by inter-clusters hydrogen bonds of **1**. Symmetry codes: (a) $x, -y, z - 1/2$; (b) $-x + 1/2, y - 1/2, z - 1$; (c) $-x + 1/2, y - 1/2, z - 2$.

structure (Fig. 3). Central Ni2 has a pentagonal bipyramid geometry formed by four $N_{acylhydrazine}$ (N1, N1a, N2 and N2a), a N_{Py} (N4), two $O_{acylhydrazine}$ (O3 and O3a) atoms in the equatorial plane, and two N_{Py} (N5 and N6) atoms locating at axial positions. However, the peripheral two Ni^{2+} ions (Ni1 and Ni1a) adopt four-coordinated square geometry completed by a $N_{acylhydrazine}$ (N1), a N_{Py} (N3), an O_{phenol} (O2) and an $O_{acylhydrazine}$ (O4) atoms. Three Ni^{2+} centers and all their donors are located in a plane, except two axial coordinated N_{Py} (N5 and N6) atoms, giving a least-square deviation of 0.133 (Fig. S1†). The torsion angle of Ni1–N–N–Ni2, Ni1···Ni2 distance and Ni1···Ni2···Ni1a angle are 177.2°, 4.728 Å and 151.9°, respectively (Table S2†). The π–π interactions are found between the ligands (Table S3†), which further link the adjacent $\{Ni_3\}$ clusters to form supramolecular chains along *b* axis (Fig. S2†).

Clusters **3** and **4** show quite similar hexanuclear structures consisting of two N–N single bonds bridged quasi-linear $\{Cu_3\}$ cores (Fig. 4), though they were assembled by different ligands, respectively. The reason is that $sphz^{6-}$ in **3** and $msphz^{6-}$ in **4** display the same μ_4-η^{11} mode (mode-III *vs.* IV, Scheme 2). Here only **3** is taken as the representative to discuss their structures in detail. Cluster **3** crystallizes in triclinic space group $P\bar{1}$. It consists of two $sphz^{6-}$ ligands, six Cu^{2+} ions, four coordinative Py and one free DMF molecules (Fig. 4a). Among six Cu^{2+} ions,

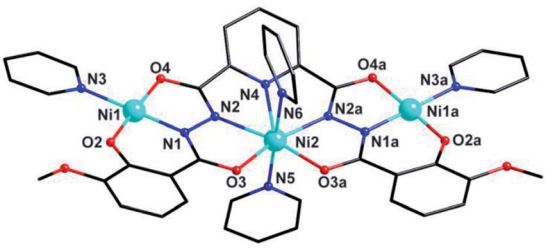

Fig. 3 Molecular structure of **2**. Symmetry codes: (a) $x, 1.5 - y, z$. Color scheme: black for C, red for O, blue for N, sky-blue for Ni.

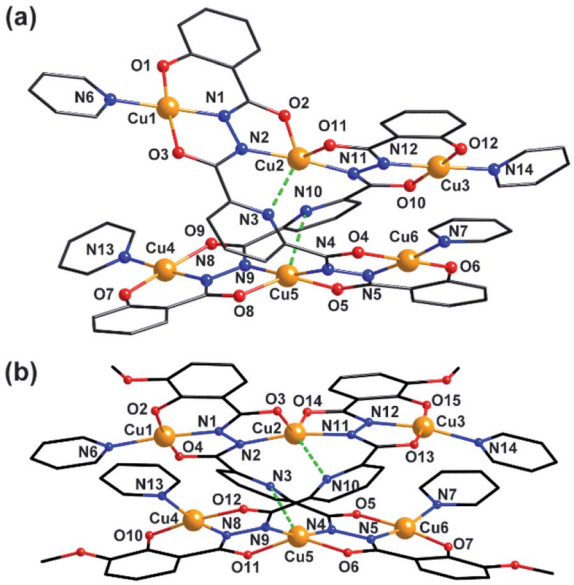

Fig. 4 Molecular structure of **3** and **4**. Color scheme: black for C, red for O, blue for N, yellow for Cu.

terminal Cu1, Cu3, Cu4 and Cu6 all display four-coordinated square geometries provided by a $N_{acylhydrazine}$ (N1, N12, N8 or N5), a N_{Py} (N6, N14, N13 or N7), an O_{phenol} (O1, O12, O7 or O6) and an $O_{acylhydrazine}$ (O3, O10, O9 or O4) atoms. While the geometries of the two central Cu^{2+} ions (Cu2 and Cu5) are distorted square pyramidal ones, as established by the calculation of geometrical parameters τ (0.47 for Cu2 and 0.25 for Cu5). Their basal planes are formed by two $N_{acylhydrazine}$ (N2 and N11 or N4 and N9), a N_{Py} (N3 or N10) and an $O_{acylhydrazine}$ (O2 or O8) atoms, and the apex are occupied by $O_{acylhydrazine}$ (O11 or O5) atoms. The Cu2–N3 and Cu5–N10 bonds are 2.671(1) and 2.882(1) Å, respectively. Both of them are much longer than those of any other Cu–N bonds in **3**, and close to the Cu–N van der Waals radii limit (2.95 Å).[17]

In contrast to nearly planar configurations of $sphz^{6-}$ in **1**, two acylhydrazine wings of each $sphz^{6-}$ in **3** twists with each other. Two such "V" shaped $sphz^{6-}$ ligands thus cross together with their notches face to face, and use their donors in notches to chelate two Cu^{2+} ions (Cu2 and Cu5) synergistically. In addition, each of four hydrozine groups also catch a Cu^{2+} ion (Cu1, Cu3, Cu4 and Cu6) with the help of O_{phenol}, with the Py as terminal ligands. In this way a hexanuclear structure that contains two discrete $\{Cu_3\}$ cores formed. Both $\{Cu_3\}$ cores show a N–N single bonds bridged quasi-linear topologies as $\{Mn_3\}$ in **1** and $\{Ni_3\}$ in **2**. However, what's different is that the two N–N bridges in each $\{Cu_3\}$ core are belonging to different $sphz^{6-}$ ligands, respectively. This dissimilarity did not lead to obvious variations in the torsion angle of M–N–N–M, M···M distances and M–M–M angle for **1–3** (Table S2†). But it makes the Cu^{2+} ions and their donors in each $\{Cu_3\}$ core form two crossed meaning planes (Fig. S1†). The least-square deviations of four meaning planes in **3** are 0.048, 0.079, 0.047 and 0.078 Å, and the twist angles of two crossing meaning planes in each $\{Cu_3\}$ core are 62.376

and 39.867°, respectively. Furthermore, due to the intermolecular π–π interactions (Table S3†) between ligands, the $\{Cu_6\}$ clusters of **3** further form supramolecular chain along *c*-axis (Fig. S3†).

Magnetic properties

The magnetic susceptibilities of **1–4** have been studied in the range of 300–2 K with an applied direct current magnetic field of 1 kOe. The room temperature $\chi_m T$ value of **1** is 10.35 cm^3 K mol^{-1}, being close to the theoretical value of 10.375 cm^3 K mol^{-1} for an uncoupled $\{Mn_2^{III}Mn^{II}\}$ system with $S(Mn^{3+}) = 2$ and $S(Mn^{2+}) = 5/2$ assuming $g = 2.00$ (Fig. 5, Table S2†). Upon cooling, the $\chi_m T$ value increases gradually, reaching the maximum of 20.44 cm^3 K mol^{-1} at 3 K, before dropping rapidly to a minimum of 19.69 cm^3 K mol^{-1} at 2 K. The Curie–Weiss fitting for the χ_m^{-1}–*T* data at the temperature range of 300–50 K gave $C = 10.28$ mol cm^{-3} and $\theta = 2.17$ K (Fig. S4†). The overall profile of $\chi_m T$–*T* curve and the positive θ are characteristic of FM coupling between Mn^{3+} and Mn^{2+} centers of **1**. While for the faster decrease of $\chi_m T$ value in the low temperature region, it may be ascribed to the presence of magnetic anisotropy zero field splitting (mainly for Mn^{3+} centers) and/or the effect of interclusters interactions.[18]

MAGPACK program[19] was used to fit magnetic interactions of **1**. On the basis of its centro-symmetric molecular structure, the magnetic interactions can be simplified as a linear trinuclear model (Fig. 5 inset) based on following Hamilton operator (eqn (1)):

$$\hat{H} = -2J(\hat{S}_1\hat{S}_2 + \hat{S}_{1a}\hat{S}_{2a}) + \sum_i \mu_B g_i \hat{S}_i \vec{H} \quad (1)$$

The *J* represents the interactions mediated by the N–N single bond pathways between the adjacent Mn centers, and the S_i is the spin vector for each Mn ion. The fitting result agrees well with the experimental data in whole temperature range (red line in Fig. 5), and gave the best parameters of $J = 5.1$ cm^{-1}, $g = 1.99$ and interclusters magnetic interactions $zJ = -0.12$ cm^{-1}. Both

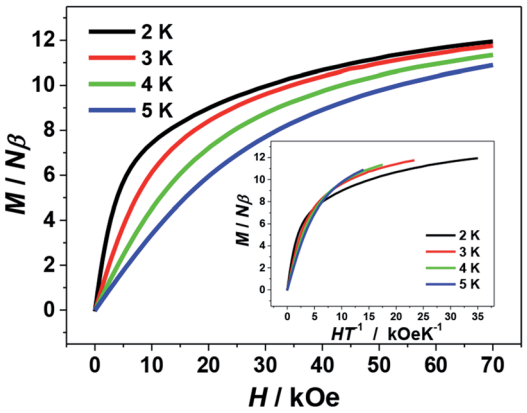

Fig. 6 Plots of *M*–*H* and *M*–HT^{-1} (inset) of **1**.

experimental and fitting results suggest a $S_T = 13/2$ spin ground state for **1** at $T = 0$ K.[7b,20]

The isothermal magnetization data for **1** were collected in the fields of 0–70 kOe at 2–5 K. As shown by the plot of *M*–*H* in Fig. 6, the magnetization value (*M*) of **1** rises rapidly from at low fields and reaches a maximum value of 11.95 Nβ at the 70 kOe at 2 K. The lack of saturation for the curve implies the appreciable magnetic anisotropy arising from the two J-T elongated peripheral Mn^{3+} ions and/or the presence of low-lying excited states of the system. This could be also supported by the plot of *M*–HT^{-1} (Fig. 6, inset), in which the curves at different temperature are not superposed. In addition, these isothermal magnetization data were also fit to investigate the zero-field splitting *D*, a parameter that related to the magnetic anisotropy of the system. However, all attempts lead to unreasonable values and/or prevent the fits from converging, which can also be seen in some other Mn clusters reported previously.[16,21]

The ac magnetic measurements of **1** were performed under zero dc fields with an ac driving field of 2.5 Oe at different frequencies. As shown in Fig. 7, cluster **1** is observed to exhibit frequency-dependent out-of-phase (χ'') ac signal at low temperature. This feature is characteristic of a superparamagnetic-like slow relaxation and thus of potential SMM

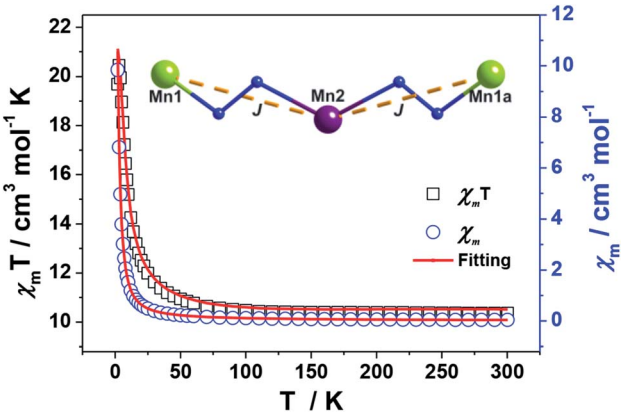

Fig. 5 Plots of $\chi_m T$–*T* and χ_m–*T* of **1**. The red lines represent the best fitting.

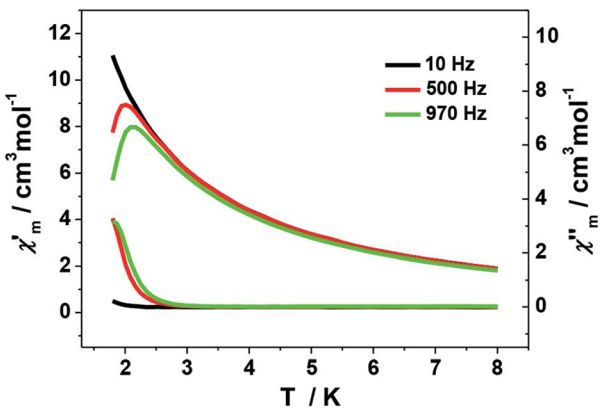

Fig. 7 Plot of the in-phase (χ') and out-of phase (χ'') ac susceptibility of **1**.

behavior. Nevertheless, it is difficult to estimate the energy barrier of **1** due to the absence of full peaks with maxima in the out-of-phase χ'' ac signal. This might be ascribed to the fast relaxation and/or small energy barrier of the system. Similar situation is commonly seen in previous Mn SMMs.[7a,b,22] In addition, the dc magnetization measurement performed at 1.8 K shows hysteresis curve with coercive field of about 50 Oe and remnant magnetization of about 0.075 Nβ (Fig. S5†).

For **2–4**, their $\chi_m T$ values at 300 K are 2.94, 2.57 and 2.29 $cm^3\ mol^{-1}$ K, respectively, which are in agreement with the expected values of 3.0 $cm^3\ mol^{-1}$ K for **2** (three uncoupled Ni^{2+} ions with $S = 1$ and $g = 2.2$) and 2.5 $cm^3\ mol^{-1}$ K for **3** and **4** (six uncoupled Cu^{2+} ions with $S = 1/2$ and $g = 2$). As the temperature was lowered, the $\chi_m T$–T values of **2–4** all show smoothly and sharply decrease in high and low temperature region successively (Fig. 8). The $\chi_m T$ values finally reach the minimum of 1.19, 0.78 and 0.59 $cm^3\ mol^{-1}$ K at 2 K, respectively. Curie–Weiss fitting afford $C = 3.15$ mol cm^{-3} and $\theta = -26.20$ K for **2**, $C = 2.76$ mol cm^{-3} and $\theta = -23.58$ K for **3** and $C = 2.37$ mol cm^{-3} and $\theta = -12.82$ K for **4** (Fig. S4†).

On account of the similar molecular structures and magnetic exchange pathways, the magnetic fitting of **2** is based on the same 2J model as that of **1** (eqn (1)). While those of **3** and **4** were modelled using following Hamiltonian (eqn (2)):

$$\hat{H} = -2J_1\hat{S}_1\hat{S}_2 - J_2\hat{S}_2\hat{S}_3 - 2J_3\hat{S}_4\hat{S}_5 - J_4\hat{S}_5\hat{S}_6 + \sum_i \mu_B g_i \hat{S}_i \vec{H} \quad (2)$$

The J_1, J_2, J_3 and J_4 are the magnetic interactions between Cu1 and Cu2, Cu2 and Cu3, Cu4 and Cu5, and Cu5 and Cu6, respectively. All these fitting data by MAGPACK support experimental results well for every system (red line in Fig. 8). The best parameters of fitting are following: $J = -12.6\ cm^{-1}$, $g = 2.2$ and $zJ = -0.18\ cm^{-1}$ for **2**, $J_1 = -5.2\ cm^{-1}$, $J_2 = -3.9\ cm^{-1}$, $J_3 = -4.7\ cm^{-1}$, $J_4 = -3.5\ cm^{-1}$, $g = 2.1$ and $zJ = -0.27\ cm^{-1}$ for **3** and $J_1 = -11.1\ cm^{-1}$, $J_2 = -9.5\ cm^{-1}$, $J_3 = -10.9\ cm^{-1}$, $J_4 = -9.1\ cm^{-1}$, $g = 2.1$ and $zJ = -0.33\ cm^{-1}$ for **4** (Table S2†). All above results indicate dominant AFM interactions between the metallic centers in each system of **2–4**.

It can be seen from the above results that the N–N single bonds in **1–4** play different roles in magnetic interactions conveying, though the trinuclear cores of **1–4** have approximately the same M–N–N–M torsion angles, M···M distances and M–M–M angles (Table S2†). Only in **1**, the N–N single bonds mediate FM interactions. This might be related to the special orbital overlaps of $Mn^{3+}\cdots Mn^{2+}$ pairs, which are different from those between the adjacent 3d metal ions of **2–4**. According to Hund's rule, the Mn^{3+} would transfer a fraction of unpaired electron from the z^2 to the $x^2 - y^2$ orbital, in order to keep the spin of the other unpaired electrons parallel to that in z^2 orbital.[23] The overlap of the magnetic orbital of an empty orbital of Mn^{3+} ions with an Mn^{2+} ion results in FM coupling on the basis of the spin polarization mechanism,[24] and thus led to a large spin ground state of **1**. Combined with the nearly perfect alignment Jahn–Teller axes of Mn^{3+} centers in its linear topology, which bring significant global anisotropy, cluster **1** finally displays SMM behavior.

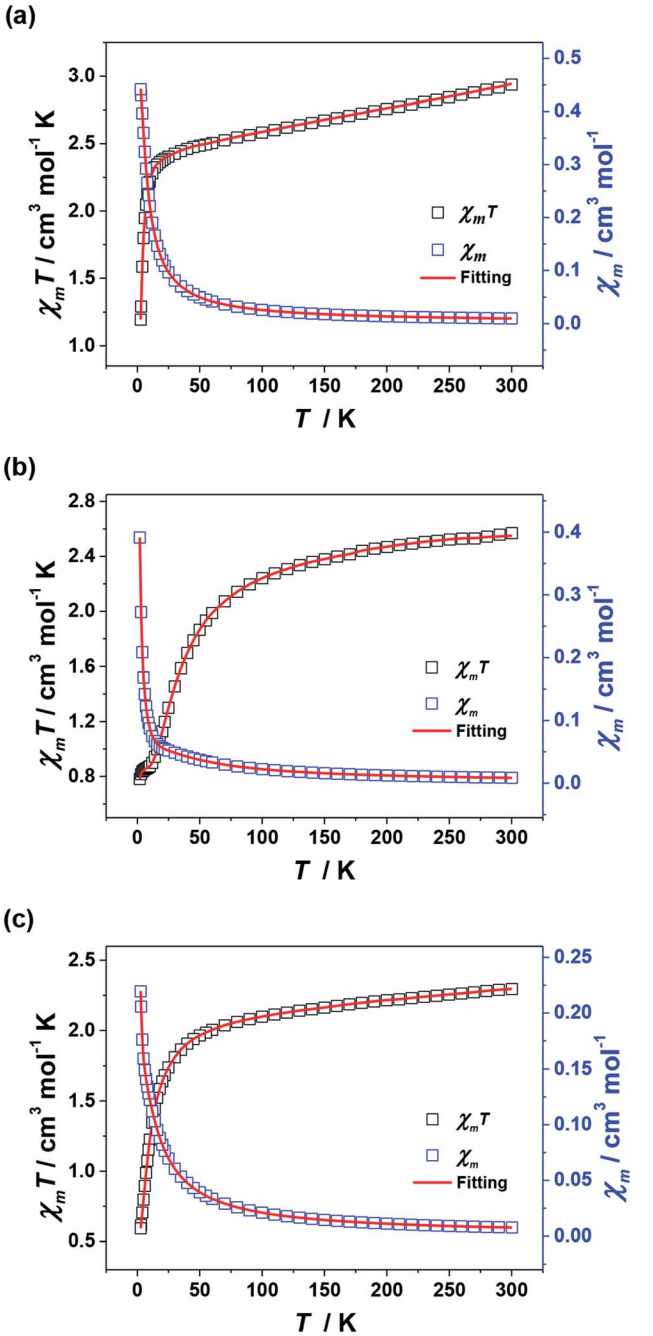

Fig. 8 Plots of $\chi_m T$–T and χ_m–T for **2** (a), **3** (b) and **4** (c). The red lines represent the best fitting.

Conclusions

In summary, we have assembled a family of novel 3d metal clusters, employing two diacylhydrazine ligands containing linearly arranged chelating pockets. They feature acylhydrazine N–N single bonds bridged quasi-linear trinuclear cores. These N–N bonds transmit FM exchange between the Mn centers in **1**, but common AFM exchanges between the adjacent 3d metal centers of **2–4**. Furthermore, cluster **1** exhibits SMM behavior. This work thus affords rare case of quasi-linear 3d SMM using

N–N single bonds as magnetic coupling pathways, and provides a new insight to the role of N–N bridges in the conveying of magnetic interactions.

Experimental

General materials and methods

All reagents were used as received without further purification. The H_4sphz and H_6msphz ligands were synthesized according to the literature.[14] IR spectra were recorded in the range of 4000–400 cm^{-1} on a Perkin-Elmer Spectrum One FT/IR spectrometer using a KBr pellet. Elemental analyses for C, H and N were carried out on a Model 2400 II, Perkin-Elmer elemental analyzer. The magnetic measurements were performed with a Quantum Design MPMS SQUIDXL-5 magnetometer equipped with a 7 T magnetic field using polycrystalline samples. Direct current (dc) magnetic susceptibility were measured in the temperature range of 300–2 K. Field-dependant magnetization plots were measured with the magnetic field varying from 0 to 7 T at the indicated temperatures. The ac susceptibility measurements were carried out with an oscillating ac field of 2.5 Oe at various frequencies at 0 Oe dc fields. The diamagnetic corrections for the complexes were estimated using Pascal's constants, and magnetic data were corrected for diamagnetic contributions of the sample holder.

Syntheses

$[Mn_2^{III}Mn^{II}(sphz)(acac)_2(CH_3OH)_4]$ (1). A mixture of $Mn(acac)_3$ (0.0352 g, 0.1 mmol), H_6sphz (0.0218 g, 0.05 mmol) in CH_3OH (10 mL) was refluxed at room temperature for 30 min followed by filtration. The filtrate was left at ambient temperature to evaporate, giving blackish crystals suitable for X-ray analysis after several days. Yield: 54% (based on ligand). Anal. calc. for $C_{35}H_{41}O_{14}N_5Mn_3$ (%): C, 45.67; H, 4.51; N, 7.69, found: C, 45.62; H, 4.45; N, 7.60. IR (KBr pellet, cm^{-1}): 3445 (s, br), 2974 (s), 1640 (w), 1453 (m), 1381 (s), 1258 (w), 1161 (w), 1059 (s), 903 (w), 840 (w), 515 (w).

$[Ni_3(msphz)(py)_4]$ (2). A mixture of $Ni(OAc)_2\cdot 4H_2O$ (0.019 g, 0.075 mmol) and H_6msphz (0.0123 g, 0.025 mmol) in 1.5 mL DMF/CH_3OH/Py (v/v/v = 1/1/1) was sealed in a Pyrex tube and heated to 70 °C for 96 h, and then cooled to room temperature at a rate of 0.5 °C min^{-1}. Reddish brown block crystals were obtained with a yield of 47% (based on ligand). Anal. calc. for $C_{43}H_{35}N_9O_8Ni_3$ (%): C, 52.60; H, 3.59; N, 12.84. Found: C, 52.78; H, 3.49; N, 12.61. IR (KBr pellet, cm^{-1}): 3423 (s, br), 3071 (m), 2830 (m), 1602 (s), 1553 (s), 1523 (s), 1459 (s), 1412 (s), 1366 (m), 1221 (m), 1079 (m), 745 (m), 691 (m).

$[Cu_6(sphz)_2(Py)_4]$ (3). A mixture of $Cu(OAc)_2\cdot 2H_2O$ (0.02 g, 0.1 mmol), H_6sphz (0.0218 g, 0.05 mmol), 4 drops Py and 4 drops trimethylacetic acid in 1.2 mL DMF/CH_3OH (v/v = 2/1) was sealed in a Pyrex tube and heated to 70 °C for 96 h, and then cooled to room temperature at a rate of 0.5 °C min^{-1}. Blackish green block crystals were obtained with a yield of 42%. Anal. calc. for $C_{69}H_{57}N_{15}O_{17}Cu_6$ (%): C, 47.37; H, 3.28; N, 12.01. Found: C, 47.65; H, 3.17; N, 11.88%. IR (KBr pellet, cm^{-1}): 3436 (s, br), 3060 (m), 2923 (m), 1665 (s), 1600 (s), 1552 (s), 1519 (s), 1453 (s), 1412 (m), 1235 (m), 1220 (m), 1073 (m), 743 (s).

$[Cu_6(msphz)_2(Py)_4]\cdot 2DMF\cdot 2H_2O$ (4). A mixture of $Cu(OAc)_2\cdot 2H_2O$ (0.015 g, 0.075 mmol) and H_6msphz (0.0123 g, 0.025 mmol) in 0.9 mL DMF/Py (v/v = 8/1) was sealed in a Pyrex tube and heated to 70 °C for 96 h, and then cooled to room temperature at a rate of 0.5 °C min^{-1}. Blackish green block crystals were obtained with a yield of 39%. Anal. calc. for $C_{71}H_{68}N_{16}O_{20}Cu_6$ (%): C, 46.18; H, 3.71; N, 12.14. Found: C, 46.65; H, 3.57; N, 11.98%. IR (KBr pellet, cm^{-1}): 3436 (s, br), 3060 (m), 2923 (m), 1665 (s), 1600 (s), 1552 (s), 1519 (s), 1453 (s), 1412 (m), 1235 (m), 1220 (m), 1073 (m), 743 (s).

X-ray structure determination

All the data for **1–4** were collected with an Agilent Supernova diffractometer by using graphite monochromatic Mo-Kα radiation ($\lambda = 0.71073$ Å). The data were collected at 296.15 (for **1**) and 150.15 K (for **2–4**), respectively. Absorption effects were corrected by semi-empirical methods. The structures were solved by direct methods and were refined by full-matrix least-squares methods with a suite of SHELX programs[25] *via* the Olex2 interface.[26] The non-hydrogen atoms were refined anisotropically. The aromatic hydrogen atoms were placed in calculated positions and refined by using a riding model, while other hydrogen atoms were located in the last final difference Fourier map. The final cycle of full-matrix least-squares refinement was based on observed reflections and variable parameters. Several severely disordered DMF and H_2O molecules in the unit cell of **4** were treated with SQUEEZE routine included in PLATON[27] during the structural refinement. Their number was estimated on the basis of the electron counts calculated by PLATON software and elemental microanalysis. A summary of crystal data and relevant refinement parameters for **1–4** are given in Table S4.† Selected bond lengths and bond angles are given in Table S5–S8.† CCDC 1496802 (**1**), 1496805 (**2**), 1496806 (**3**) and 1496807 (**4**) contain the supplementary crystallographic data for this paper.

Conflicts of interest

There are no conflicts to declare.

Acknowledgements

This work is supported by the National Natural Science Foundation of China (Grant No. 51572050), the Guangxi Natural Science Foundation (Grant No. 2015GXNSFDA139007), and Scientific Research Staring Foundation of Guilin University of Technology (Grant No. GUTQDJJ20172016028). We thank the supported from the Program of the Collaborative Innovation Center for Exploration of Hidden Nonferrous Metal Deposits and Development of New Materials in Guangxi (No. GXYSXTZX2017-II-3).

Notes and references

1 (*a*) R. Sessoli, D. Gatteschi, A. Caneschi and M. A. Novak, *Nature*, 1993, **365**, 141; (*b*) M. Murrie, *Chem. Soc. Rev.*, 2010, **39**, 1986; (*c*) K. Liu, X. J. Zhang, X. X. Meng, W. Shi, P. Cheng and A. K. Powell, *Chem. Soc. Rev.*, 2016, **45**, 2423.

2 (*a*) P. Zhang, Y. N. Guo and J. K. Tang, *Coord. Chem. Rev.*, 2013, **257**, 1728; (*b*) G. A. Timco, E. J. L. McInnes and R. E. P. Winpenny, *Chem. Soc. Rev.*, 2013, **42**, 1796; (*c*) C. Papatriantafyllopoulou, E. E. Moushi, G. Christou and A. J. Tasiopoulos, *Chem. Soc. Rev.*, 2016, **45**, 1597.

3 (*a*) G. E. Kostakis, A. M. Ako and A. K. Powell, *Chem. Soc. Rev.*, 2010, **39**, 2238; (*b*) A. Vinslava, A. J. Tasiopoulos, W. Wernsdorfer, K. A. Abboud and G. Christou, *Inorg. Chem.*, 2016, **55**, 3419.

4 (*a*) S. L. Castro, Z. Sun, C. M. Grant, J. C. Bollinger, D. N. Hendrickson and G. Christou, *J. Am. Chem. Soc.*, 1998, **120**, 2365; (*b*) Y. Y. Zhu, T. T. Yin, S. D. Jiang, A. Barra, W. Wernsdorfer, P. Neugebauer, R. Marx, M. Dörfel, B. W. Wang, Z. Q. Wu, J. Slageren and S. Gao, *Chem. Commun.*, 2014, **50**, 15090; (*c*) J. D. Leng, S. K. Xing, R. Herchel, J. L. Liu and M. L. Tong, *Inorg. Chem.*, 2014, **53**, 5458; (*d*) G. Aromí, S. Parsons, W. Wernsdorfer, E. K. Brechin and E. J. L. McInnes, *Chem. Commun.*, 2005, 5038; (*e*) C. J. Milios, A. Vinslava, P. A. Wood, S. Parsons, W. Wernsdorfer, G. Christou, S. P. Perlepes and E. K. Brechin, *J. Am. Chem. Soc.*, 2007, **129**, 8; (*f*) A. Tomsa, J. Martínez-Lillo, Y. L. Li, L. Chamoreau, K. Boubekeur, F. Farias, M. A. Novak, E. Cremades, E. Ruiz, A. Proust, M. Verdaguer and P. Gouzerh, *Chem. Commun.*, 2010, **46**, 5106.

5 (*a*) G. Aromi and E. K. Brechin, *Struct. Bonding*, 2006, **122**, 1; (*b*) A. J. Tasiopoulos and S. P. Perlepes, *Dalton Trans.*, 2008, 5537; (*c*) A. Das, K. Gieb, Y. Krupskaya, S. Demeshko, S. Dechert, R. Klingeler, V. Kataev, B. Büchner, P. Müller and F. Meyer, *J. Am. Chem. Soc.*, 2011, **133**, 3433.

6 K. Y. Monakhov, J. van Leusen, P. Kçgerler, E. L. Zins, M. E. Alikhani, M. Tromp, A. A. Danopoulos and P. Braunstein, *Chem.–Eur. J.*, 2017, **23**, 6504.

7 (*a*) A. Prescimone, J. Wolowska, G. Rajaraman, S. Parsons, W. Wernsdorfer, M. Murugesu, G. Christou, S. Piligkos, E. J. L. McInnes and E. K. Brechin, *Dalton Trans.*, 2007, 5282; (*b*) P. H. Lin, S. Gorelsky, D. Savard, T. J. Burchell, W. Wernsdorfer, R. Clérac and M. Murugesu, *Dalton Trans.*, 2010, **39**, 7650; (*c*) C. L. Zhou, Z. M. Wang, B. W. Wang and S. Gao, *Dalton Trans.*, 2012, **41**, 13620; (*d*) D. C. Li, H. S. Wang, S. N. Wang, Y. P. Pan, C. J. Li, J. M. Dou and Y. Song, *Inorg. Chem.*, 2010, **49**, 3688.

8 (*a*) Y. Z. Zhang, A. J. Brown, Y. S. Meng, H. L. Sun and S. Gao, *Dalton Trans.*, 2015, **44**, 2865; (*b*) Y. Z. Zheng, M. Speldrich, H. Schilder, X. M. Chen and P. Kögerler, *Dalton Trans.*, 2010, **39**, 10827; (*c*) D. Y. Wu, X. X. Zhang, P. Huang, W. Huang, M. Y. Ruan and Z. W. Ouyang, *Inorg. Chem.*, 2013, **52**, 10976.

9 (*a*) C. Papatriantafyllopoulou, S. Zartilas, M. J. Manos, C. Pichon, R. Clérac and A. J. Tasiopoulos, *Chem. Commun.*, 2014, **50**, 14873; (*b*) Y. Z. Zhang, U. P. Mallik, N. P. Rath, R. Clérac and S. M. Holmes, *Inorg. Chem.*, 2011, **50**, 10537; (*c*) T. N. Nguyen, W. Wernsdorfer, M. Shiddiq, K. A. Abboud, S. Hillc and G. Christou, *Chem. Sci.*, 2016, **7**, 1156; (*d*) Y. F. Zeng, X. Hu, F. C. Liu and X. H. Bu, *Chem. Soc. Rev.*, 2009, **38**, 469.

10 (*a*) H. Yang, F. Cao, D. C. Li, S. Y. Zeng, Y. Song and J. M. Dou, *Dalton Trans.*, 2015, **44**, 6620; (*b*) E. C. Yang, Z. Y. Liu, L. Zhang, N. Yang and X. J. Zhao, *Dalton Trans.*, 2016, **45**, 8134; (*c*) X. B. Li, G. M. Zhuang, X. Wang, K. Wang and E. Q. Gao, *Chem. Commun.*, 2013, **49**, 1814.

11 (*a*) S. T. Wu, H. L. Tang, S. M. Lu, Q. Y. Ye, X. H. Huang, C. C. Huang, X. L. Hu and S. T. Zheng, *CrystEngComm*, 2014, **16**, 9792; (*b*) L. K. Thompsona and L. N. Dawe, *Coord. Chem. Rev.*, 2015, **289–290**, 13.

12 Z. Q. Xu, L. K. Thompson, D. O. Miller, H. J. Clase, J. A. K. Howard and A. E. Goeta, *Inorg. Chem.*, 1998, **37**, 3620.

13 (*a*) K. Wang, Z. L. Chen, H. H. Zou, K. Hu, H. Y. Li, Z. Zhang, W. Y. Sun and F. P. Liang, *Chem. Commun.*, 2016, **52**, 8297; (*b*) Z. L. Chen, S. N. Qin, D. C. Liu, Y. L. Shen and F. P. Liang, *Cryst. Growth Des.*, 2013, **13**, 3389; (*c*) Z. L. Chen, Y. L. Shen, L. L. Li, H. H. Zou, X. X. Fu, Z. Y. Liu, K. Wang and F. P. Liang, *Dalton Trans.*, 2017, **46**, 15032.

14 (*a*) S. N. Qin, Z. L. Chen, D. C. Liu, W. Y. Huang and F. P. Liang, *Inorg. Chem. Commun.*, 2011, **14**, 784; (*b*) K. Wang, X. K. Huang, L. Zhu, Z. L. Chen and F. P. Liang, *Chin. J. Struct. Chem.*, 2016, **35**, 1912.

15 N. E. Brese and M. O'keeffe, *Acta Crystallogr.*, 1991, **B47**, 192.

16 F. Habib, G. Brunet, F. Loiseau, T. Pathmalingam, T. J. Burchell, A. M. Beauchemin, W. Wernsdorfer, R. Clerac and M. Murugesu, *Inorg. Chem.*, 2013, **52**, 1296.

17 P. M. Cheung, R. F. Berger, L. N. Zakharov and J. D. Gilbertson, *Chem. Commun.*, 2016, **52**, 4156.

18 A. Jana, N. Aliaga-Alcalde, E. Ruiz and S. Mohanta, *Inorg. Chem.*, 2013, **52**, 7732.

19 (*a*) J. J. Borrás-Almenar, J. M. Clemente-Juan, E. Coronado and B. S. J. Tsukerblat, *Inorg. Chem.*, 1999, **38**, 6081; (*b*) J. J. Borrás-Almenar, J. M. Clemente-Juan, E. Coronado and B. S. J. Tsukerblat, *Comput. Chem.*, 2001, **22**, 985.

20 A. M. Ako, I. J. Hewitt, V. Mereacre, R. Clerac, W. Wernsdorfer, C. E. Anson and A. K. Powell, *Angew. Chem., Int. Ed.*, 2006, **45**, 4926.

21 (*a*) C. J. Milios, R. Inglis, L. F. Jones, A. Prescimone, S. Parsons, W. Wernsdorfer and E. K. Brechin, *Dalton Trans.*, 2009, 2812; (*b*) M. J. H. Ojea, M. A. Hay, G. Cioncoloni, G. A. Craig, C. Wilson, T. Shiga, H. Oshio, M. D. Symes and M. Murrie, *Dalton Trans.*, 2017, **46**, 11201.

22 (*a*) T. N. Nguyen, M. Shiddiq, T. Ghosh, K. A. Abboud, S. Hill and G. Christou, *J. Am. Chem. Soc.*, 2015, **137**, 7160; (*b*) T. N. Nguyen, W. Wernsdorfer, K. A. Abboud and G. Christou, *J. Am. Chem. Soc.*, 2011, **133**, 20688.

23 T. Glaser, *Chem. Commun.*, 2011, **47**, 116, and references therein.

24 H. Liu, J. L. Tian, Y. Y. Kou, J. Y. Zhang, L. Feng, D. D. Li, W. Gu, X. Liu, D. Z. Liao, P. Cheng, J. Ribas and S. P. Yan, *Dalton Trans.*, 2009, 10511.

25 (*a*) G. M. Sheldrick, *Acta Crystallogr.*, 2008, **A64**, 112; (*b*) G. M. Sheldrick, *Acta Crystallogr.*, 2015, **C71**, 3.

26 O. V. Dolomanov, L. J. Bourthis, R. L. Gildea, J. A. K. Howard and H. J. Puschmann, *Appl. Crystallogr.*, 2009, **42**, 339.

27 A. L. Spek, *J. Appl. Crystallogr.*, 2003, **36**, 7.

